Integrated Optical Pressure Sensors in Silicon-on-Insulator
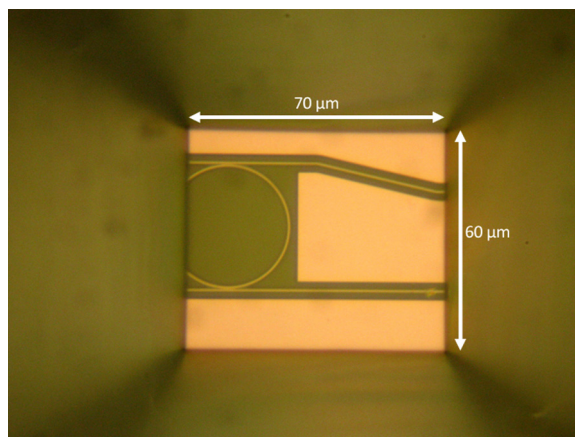
E. Hallynck, Student Member, IEEE
P. Bienstman, Member, IEEE

Integrated Optical Pressure Sensors in Silicon-on-Insulator

E. Hallynck,[1,2] *Student Member, IEEE*, **and P. Bienstman,**[1,2] *Member, IEEE*

[1]Photonics Research Group, Department of Information Technology,
Ghent University—IMEC, 9000 Gent, Belgium
[2]Center for Nano- and Biophotonics (NB-Photonics), Ghent University, 9000 Gent, Belgium

Abstract: An optical pressure sensor can be useful in many applications where electronics fall short (e.g., explosive environments). We have fabricated and characterized compact, integrated optical pressure sensors on a silicon-on-insulator platform using ring resonators and Mach–Zehnder interferometers. The silicon substrate is locally etched using KOH to produce very thin membranes of 3.28 μm. Measurements have shown that spectral features in our devices can shift up to 370 pm going from 0 to 80 kPa.

Index Terms: Nanophotonics, optoelectronic and photonic sensor, photonic integrated circuits.

1. Introduction

Checking the quality of a vacuum, controlling tire pressure, or determining the altitude in an airplane: These are all applications for a pressure sensor. For decades, research into electrical pressure sensors has been ongoing with plenty of scientific output [1]–[3]. Although most sensors focus on an electrical implementation, there is also a possibility to develop the sensor in the optical domain where the key advantages are that optical devices are immune to electromagnetic interference and can be deployed in explosive or spark-sensitive environments. Indeed, a lot of work has been published about these optical pressure sensors [4]–[17]. Optical pressure sensors can be subdivided into two main categories: integrated and nonintegrated sensors. Nonintegrated sensors consist of several discrete components that, in some cases, require precise alignment, which can increase the packaging cost drastically. Well-known examples of nonintegrated pressure sensors are Fabry–Perot based sensors [4]–[7]. Integrated sensors can be subdivided into two categories: sensors where the transducer is integrated but source and detector are external (e.g., fiber Bragg grating based sensors [8]–[12]) and sensors where source, transducer, and detector are fully integrated. Fully integrated optical pressure sensors have already been demonstrated in a variety of material platforms [13]–[17], but here, we demonstrate such a sensor in a silicon-on-insulator platform, the main advantage of which is mass fabrication of devices at a low cost.

2. Operation Principle

The operation principle of the optical pressure sensor described here is as follows: The substrate under part of a ring resonator or Mach–Zehnder interferometer on a chip is locally thinned in order to achieve a pressure-sensitive membrane. When applying a differential pressure on the membrane, the structure will deform according to the nonlinear Föppl-von Kármán equations [18] in (1), where E is
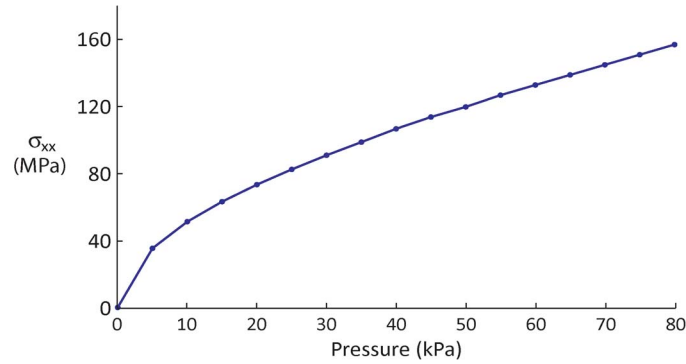
Fig. 1. Nonlinear response of the in plane stress σ_{xx} in the center of the membrane to the applied pressure.

Young's modulus, h is the plate thickness, ν is Poisson's ratio, ζ is the out of plane deflection, $\sigma_{\alpha\beta}$ is the stress tensor with $\alpha = 1-3$ and $\beta = 1-3$ (corresponding to x, y, and z), and P is the applied pressure

$$\frac{Eh^3}{12(1-\nu^2)}\Delta^2\zeta - h\frac{\partial}{\partial x_\beta}\left(\sigma_{\alpha\beta}\frac{\partial\zeta}{\partial x_\alpha}\right) = P$$

$$\frac{\partial\sigma_{\alpha\beta}}{\partial x_\beta} = 0. \tag{1}$$

The resulting membrane deformation will induce stress which, in turn, causes the elastooptic effect [19] to alter the optical path length of the light in the structure according to (2), where $(1/n^2)_i$ are the components of the indicatrix, π_{ik} are the piezooptical coefficients, and σ_k are the stress components with $i = 1-6$ and $k = 1-6$, where $1 \equiv xx$, $2 \equiv yy$, $3 \equiv zz$, $4 \equiv yz$, $5 \equiv xz$, and $6 \equiv xy$

$$\Delta\left(\frac{1}{n^2}\right)_i = \sum_{k=1}^{6}\pi_{ik}\sigma_k. \tag{2}$$

This gives rise to a phase shift $\Delta\phi$ as shown in (3), where λ is the wavelength of the incident light, and $n_{eff}(l)$ is the local effective index along the waveguides of the structure located on the membrane. This, in turn, will shift the position of the spectral features in the wavelength spectrum. Measuring this shift gives an indication on how much the pressure has changed

$$\Delta\phi = \frac{2\pi}{\lambda}\int_{waveguide} n_{eff}(l)\mathrm{d}l. \tag{3}$$

Solving the Föppl-von Kármán equations analytically is not possible. Therefore, we have used the finite elements solver ANSYS [20] to determine the stress caused by pressure in a 60 μm by 60 μm, 220-nm-thin silicon membrane. As can be seen from Fig. 1 we observe a nonlinear response of the in plane stress σ_{xx} in the center of the membrane to the applied pressure.

3. Experiments

3.1. Device Description

The photonic structures are fabricated using a 193-nm-deep ultraviolet lithography process on a silicon-on-insulator wafer comprising 220 nm silicon on 2 μm silicon dioxide on a 750-μm silicon substrate [21]. After lithography and etching of the structures, the substrate is thinned down to a thickness of 250 μm and diced into smaller dies. After this, we deposit a stack of 600 nm plasma enhanced chemical vapor deposited (PECVD) silicon nitride on 600 nm PECVD silicon dioxide on the back side of the sample; these layers will serve as an etching mask for silicon wet etching using
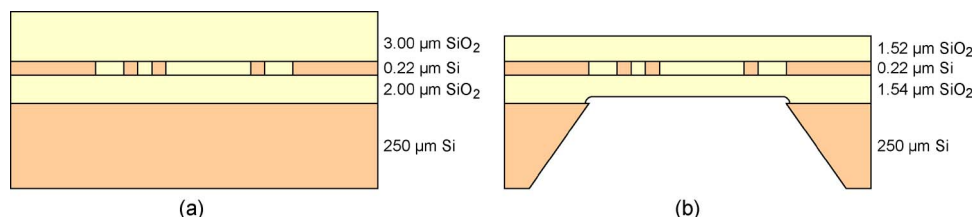
Fig. 2. (a) Initial and (b) final layer stack of the pressure-sensitive membrane.
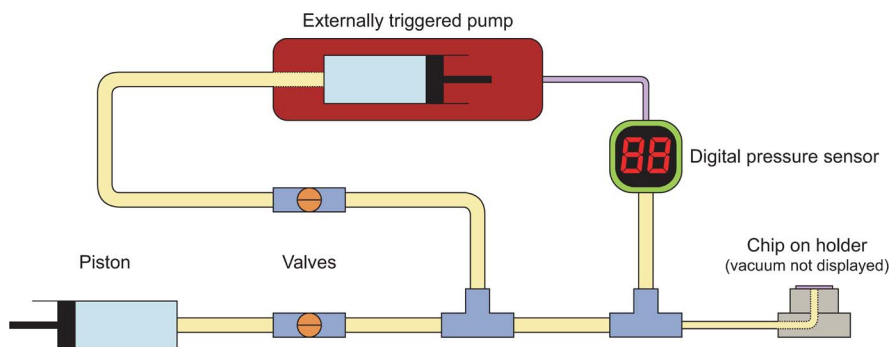

Fig. 3. Pressure is applied to the sample on a dedicated holder using a piston. A feedback mechanism is included to prevent the pressure from leaking away.

KOH. The silicon dioxide deposited as a buffer layer to minimize stress-induced effects (which degrade the mask quality) due to the lattice mismatch between silicon and silicon nitride. On the top side, we deposit 3000 nm PECVD silicon dioxide to protect the light guiding silicon structures in the 220-nm silicon layer. We perform contact lithography on the back side of the sample using alignment markers located on the top of the sample. Using reactive ion etching, windows are opened in the silicon nitride mask and silicon dioxide buffer layer. Since the silicon dioxide can contain pinholes that allow the KOH to damage the structures, we spincoat the commercially available ProTEK [22] on the top side of the sample as an extra protective coating. Now that the layer stack is complete, we put the sample in 20% KOH for approximately 3 h at 79 °C. KOH etches the silicon substrate anisotropically until it practically stops at the silicon dioxide layer. After etching, we remove the ProTEK layer and any other residues using both a piranha solution and oxygen plasma. A 40-s dip in 49% HF removes part of the silicon oxide layers to further thin down the membranes. According to SEM measurements, the membranes consist of 1.52 μm PECVD silicon dioxide on 220 nm silicon on 1.54 μm buried silicon dioxide, bringing the total membrane thickness to 3.28 μm (see Fig. 2).

3.2. Setup Description

To characterize the devices in the wavelength spectrum, we use a Santec TSL-510 tunable laser coupled to an optical fiber. Using a grating coupler [23], the light mode in the fiber is coupled to the TE mode of a silicon single mode waveguide in the top silicon layer. The light then enters the transducer (i.e., ring resonator or Mach–Zehnder interferometer on a membrane) and is coupled out again using another grating coupler. The light is collected using an optical fiber and fed to an HP 8153A Optical power meter. As illustrated in Fig. 3, we designed a special mechanical chuck with which we can apply a pressure difference while keeping the sample in position using vacuum. The pressure difference is generated by changing the volume—by means of a piston—of a pressure circuit that is on one end closed by the membrane of our chip. The top side of the membrane is always subject to atmospheric pressure. To ensure that we maintain a fixed pressure, we include a
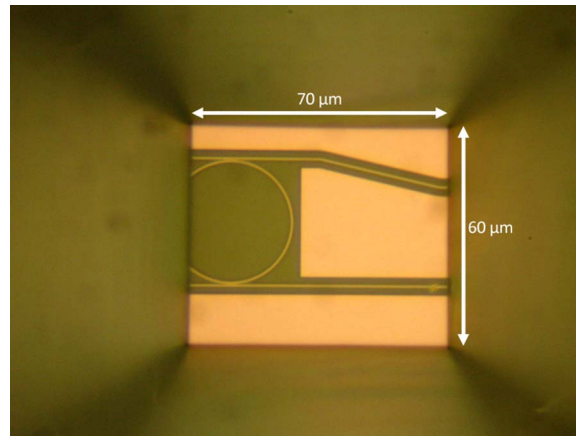
Fig. 4. Microscope image of an underetched ring resonator on a membrane, seen through a hole in the substrate. Dimensions are 60 μm $\times$ 70 μm (length $\times$ width).
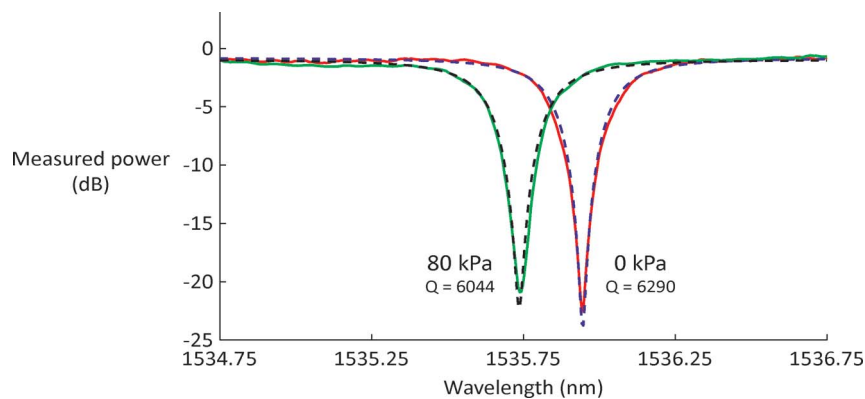

Fig. 5. Measurements of a resonance of a ring resonator are shown here (solid line) along with their fitted Lorentzian shape (dashed line) for a pressure of 0 kPa and 80 kPa. A clear shift is visible with only very slight degradation of the quality factor.

feedback mechanism; a digital pressure sensor triggers a pump when the pressure is about to drop below a certain level. Due to the design of the sample holder, we are unable to apply positive pressure (i.e., pressure in the circuit greater than atmospheric pressure) since the applied pressure would try to lift the sample upwards, thus opening the closed pressure circuit. Future designs of this holder should clamp the sample mechanically as to allow positive pressure to be applied to the sample. For all characterized devices, an intensity peak in the vicinity of 1.55 μm is selected to be monitored. A 2-nm window around this peak is then swept using the tunable laser with a step size of 5 pm. A negative pressure of 80 kPa is applied, and the shifted position of the peak is determined. The negative pressure value is then decreased in steps of generally 10 kPa, and this is continued until the pressure difference reaches 0 again. Data analysis consists of fitting a Lorentzian shape [24], in the case of ring resonators, or a squared cosine [13], in the case of Mach–Zehnder interferometers, to the measurements.

3.3. Measurements

The first structure we will highlight is a ring resonator, as shown in Fig. 4. Conventionally, only part of the ring resonator is underetched [16], but due to suboptimal alignment accuracy in our contact lithography, we opted for a larger membrane that holds almost the entire structure. Fig. 5
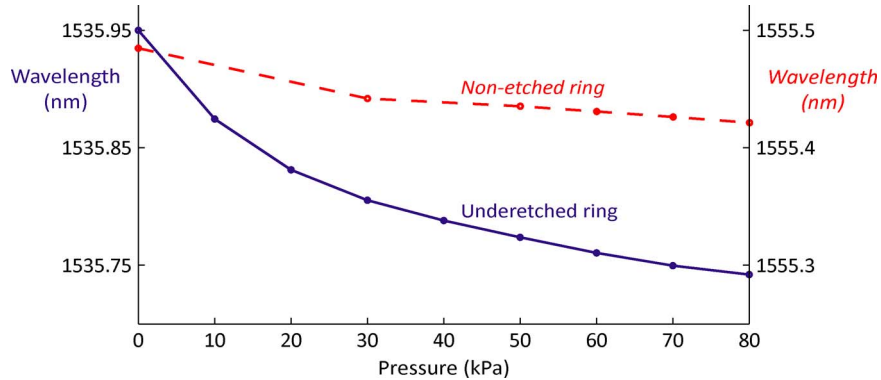
Fig. 6. Resonance position in function of pressure of a ring resonator membrane. A nonetched ring in the vicinity of the membrane also reacts to the pressure difference, albeit in a less-sensitive manner. The total shift from 0 to 80 kPa for an etched and nonetched ring is, respectively, 208 pm and 62 pm.

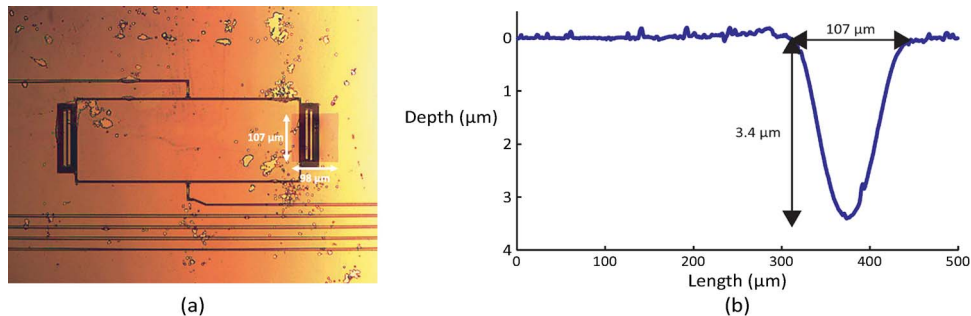(a)   (b)

Fig. 7. (a) Microscope image of a Mach–Zehnder interferometer with two waveguide spiral arms as seen from the top side. The right arm is underetched and acts as a pressure-sensitive membrane with dimensions of 107 μm × 98 μm (length × width). (b) Measurement of the buckling depth using a Dektak profilometer (buckling depth is 3.4 μm).

shows indeed that the spectral position of a resonance in the ring resonator shifts under the influence of pressure. As can be seen in Fig. 6, the position of the resonance peak is nonlinearly related to the applied pressure, and we observe a similar curve, as in Fig. 1. Due to the complex shape of the ring resonator, it is, however, not straightforward to perform an exact fitting to our measurement data.

Going from 0 to 80 kPa, the position of the resonance shifts by 208 pm. It should, however, be noted that the resonances in nonetched ring resonators also undergo a spectral shift when applying pressure (a phenomenon that can already be verified by applying vacuum to the back of a sample). We measured a ring resonator with similar dimensions as the one in Fig. 4 and found the shift from 0 to 80 kPa to be 62 pm, which is significantly less than that of the etched variant. In this case, the applied pressure does not act on a membrane but on the entire thinned sample, causing enough stress to induce a noticeable resonance shift. It is also worth mentioning that the quality factor of the resonance and overall transmission only degrades very slightly when applying pressure (see also Fig. 5).

As mentioned above, a Mach–Zehnder interferometer can also be used for sensing. Fig. 7 shows part of the device we have investigated. In this case, one of the arms of the Mach–Zehnder interferometer is partly underetched. The slight discoloring in the picture indicates buckling [25] of the membrane due to stress from the silicon dioxide layers. Using a Dektak profilometer, we measured the buckling depth and found it to be 3.4 μm. Despite this undesired buckling behavior,
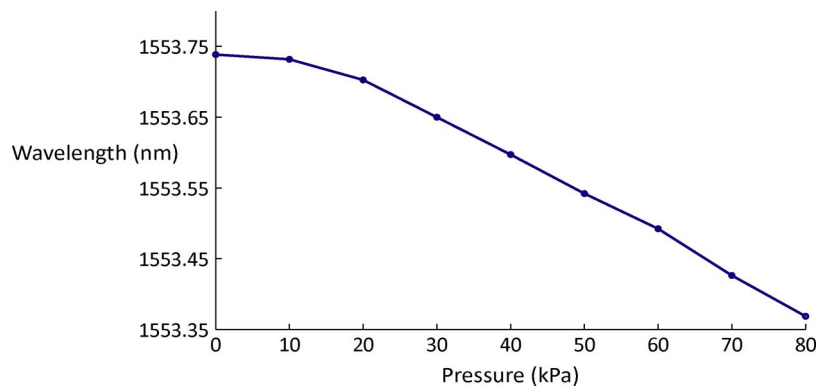
Fig. 8. Position of a spectral dip in function of the pressure applied to a Mach–Zehnder interferometer on a membrane. The total shift from 0 to 80 kPa is 370 pm.

some devices still show spectral features that shift under influence of pressure, the results of which are shown in Fig. 8. The response is, however, different from that of the ring resonator (see Fig. 6), which we believe is caused by the buckling. The total shift at a pressure of 80 kPa is 370 pm.

4. Discussion

When comparing the ring resonator and Mach–Zehnder interferometer, we can state that although the ring resonator shows slightly less sensitivity, it not only requires a smaller footprint—a Mach–Zehnder always needs a reference arm—but it also exhibits sharper resonant features, which benefits the resolution of readout. An advantage of the Mach–Zehnder interferometer is that, when suitably designed, it can show a reduced temperature dependence.

Although the above structures already show a high sensitivity, considering their small footprint, there is still room for improvement. It has been shown that a membrane where the length/width ratio equals 2 will exhibit higher sensitivity [14]. Second, increased performance is expected when more accurate alignment allows for precise placement of the sensing arms on the membrane. Moreover, in [14] and [16], it is shown that using TM polarized light will enhance the sensitivity since the refractive index change in the out-of-plane direction is greater than it is in plane. Finally, the membranes can be thinned down further using HF or dry etching to achieve more sensitive devices. It should, however, be noted that stress induced by silicon dioxide can cause some membranes to buckle, unless the sensor size is decreased. This problem can, however, be circumvented by placing several smaller sensors in series, as demonstrated by [13].

5. Conclusion

In conclusion, we have demonstrated pressure sensors in silicon-on-insulator with a relatively thin pressure-sensitive membrane (3.28 μm). This material platform allows for cheap mass fabrication of the proposed devices. Although the light source and the detector are connected to the sensor using fibers in this experiment, there are no factors that would prevent complete integration of source, transducer, and detector on one single chip. The high refractive index contrast in silicon-on-insulator, combined with the small membrane thickness, permits us to fabricate highly sensitive sensors with a small footprint (the smallest of our devices measuring 60 μm $\times$ 70 μm). Due to the nonlinear response of the sensor, it is not straightforward to determine a sensitivity per unit of pressure, but a shift of spectral features of up to 370 pm for a differential pressure of 80 kPa has been demonstrated, which is in the same order of magnitude as in [13], where much larger membranes are used (order of millimeters). Furthermore, we are confident that future design and fabrication improvements will help increase this number.

Acknowledgment

References

[1] V. Mortet, R. Petersen, K. Haenen, and M. D'Olieslaeger, "Wide range pressure sensor based on a piezoelectric bimorph microcantilever," *Appl. Phys. Lett.*, vol. 88, no. 13, p. 133511, Mar. 2006. [Online]. Available: http://link.aip.org/link/APPLAB/v88/i13/p133511/s1&Agg=doi

[2] I. Manunza, A. Sulis, and A. Bonfiglio, "Pressure sensing by flexible, organic, field effect transistors," *Appl. Phys. Lett.*, vol. 89, no. 14, p. 143 502, Oct. 2006. [Online]. Available: http://link.aip.org/link/APPLAB/v89/i14/p143502/s1&Agg=doi

[3] M. A. Fonseca, J. M. English, M. von Arx, and M. G. Allen, "Wireless micromachined ceramic pressure sensor for high-temperature applications," *J. Microelectromech. Syst.*, vol. 11, no. 4, pp. 337–343, Aug. 2002.

[4] W. Wang, N. Wu, Y. Tian, C. Niezrecki, and X. Wang, "Miniature all-silica optical fiber pressure sensor with an ultrathin uniform diaphragm," *Opt. Exp.*, vol. 18, no. 9, pp. 9006–9014, Apr. 2010. [Online]. Available: http://www.ncbi.nlm.nih.gov/pubmed/20588746

[5] W. Wang, N. Wu, Y. Tian, X. Wang, C. Niezrecki, and J. Chen, "Optical pressure/acoustic sensor with precise Fabry–Perot cavity length control using angle polished fiber," *Opt. Exp.*, vol. 17, no. 19, pp. 16613–16618, Sep. 2009. [Online]. Available: http://www.ncbi.nlm.nih.gov/pubmed/19770876

[6] I. Padron, A. T. Fiory, and N. M. Ravindra, "Integrated optical and electronic pressure sensor," *IEEE Sens. J.*, vol. 11, no. 2, pp. 343–350, Feb. 2011.

[7] F. Xu, D. Ren, X. Shi, C. Li, W. Lu, L. Lu, L. Lu, and B. Yu, "High-sensitivity Fabry–Perot interferometric pressure sensor based on a nanothick silver diaphragm," *Opt. Lett.*, vol. 37, no. 2, pp. 133–135, Jan. 2012.

[8] H.-J. Sheng, M.-Y. Fu, T.-C. Chen, W.-F. Liu, and S.-S. Bor, "A lateral pressure sensor using a fiber Bragg grating," *IEEE Photon. Technol. Lett.*, vol. 16, no. 4, pp. 1146–1148, Apr. 2004.

[9] B. McMillen, C. Jewart, M. Buric, K. P. Chen, Y. Lin, and W. Xu, "Fiber Bragg grating vacuum sensors," *Appl. Phys. Lett.*, vol. 87, no. 23, p. 234 101, Dec. 2005. [Online]. Available: http://link.aip.org/link/APPLAB/v87/i23/p234101/s1&Agg=doi

[10] X. Ni, Y. Zhao, and J. Yang, "Research of a novel fiber Bragg grating underwater acoustic sensor," *Sens. Actuators A, Phys.*, vol. 138, no. 1, pp. 76–80, Jul. 2007. [Online]. Available: http://linkinghub.elsevier.com/retrieve/pii/S0924424707003457

[11] S. Campopiano, A. Cutolo, A. Cusano, M. Giordano, G. Parente, G. Lanza, and A. Laudati, "Underwater acoustic sensors based on fiber Bragg gratings," *Sensors*, vol. 9, no. 6, pp. 4446–4454, Jun. 2009. [Online]. Available: http://www.mdpi.com/1424-8220/9/6/4446/

[12] D. A. Singlehurst, C. R. Dennison, and P. M. Wild, "Comprising multiplexed in-Fibre Bragg gratings within a flexible superstructure," *J. Lightw. Technol.*, vol. 30, no. 1, pp. 123–129, 2012.

[13] H. Porte, V. Gorel, S. Kiryenko, J.-P. Goedgebuer, W. Daniau, and P. Blind, "Imbalanced Mach–Zehnder interferometer integrated in micromachined silicon substrate for pressure sensor," *J. Lightw. Technol.*, vol. 17, no. 2, pp. 229–233, Feb. 1999. [Online]. Available: http://ieeexplore.ieee.org/lpdocs/epic03/wrapper.htm?arnumber=744229

[14] M. Ohkawa, M. Izutsu, and T. Sueta, "Integrated optic pressure sensor on silicon substrate," *Appl. Opt.*, vol. 28, no. 23, pp. 5153–5157, Dec. 1989. [Online]. Available: http://www.ncbi.nlm.nih.gov/pubmed/20556016

[15] C. Wagner, J. Frankenberger, and P. Deimel, "Optical pressure sensor based on a Mach–Zehnder interferometer integrated with a lateral a-Si:H p-i-n photodiode," *IEEE Photon. Technol. Lett.*, vol. 5, no. 10, pp. 1257–1259, Oct. 1993. [Online]. Available: http://ieeexplore.ieee.org/lpdocs/epic03/wrapper.htm?arnumber=248446

[16] G. de Brabander, J. Boyd, and G. Beheim, "Integrated optical ring resonator with micromechanical diaphragms for pressure sensing," *IEEE Photon. Technol. Lett.*, vol. 6, no. 5, pp. 671–673, May 1994. [Online]. Available: http://ieeexplore.ieee.org/lpdocs/epic03/wrapper.htm?arnumber=285575

[17] P. K. Pattnaik, B. Vijayaaditya, T. Srinivas, and A. Selvarajan, "Optical MEMS pressure sensor using ring resonator on a circular diaphragm," in *Proc. ICMENS*, 2005, pp. 1–4.

[18] L. D. Landau, E. M. Lifshitz, A. M. Kosevich, and L. P. Pitaevskii, *Theory of Elasticity*. Oxford, U.K.: Butterworth-Heinemann, 1986.

[19] C. C. Davis, "The electrooptic and acoustooptic effects and modulation of light beams," in *Lasers and Electro-Optics*. Cambridge, U.K.: Cambridge Univ. Press, 1996, pp. 623–639.

[20] ANSYS, ANSYS Mechanical APDL. [Online]. Available: http://www.ansys.com/

[21] S. K. Selvaraja, P. Jaenen, W. Bogaerts, D. V. Thourhout, P. Dumon, and R. Baets, "Fabrication of photonic wire and crystal circuits in silicon-on-insulator using 193 nm optical lithography," *J. Lightw. Technol.*, vol. 27, no. 18, pp. 4076–4083, Sep. 2009.

[22] Brewer Science, Wet-Etch Protective Coatings—ProTEK B3. [Online]. Available: http://www.brewerscience.com/products/protective-coatings/wet-etch-protective-coating/

[23] D. Taillaert, W. Bogaerts, P. Bienstman, T. F. Krauss, P. V. Daele, I. Moerman, S. Verstuyft, K. D. Mesel, and R. Baets, "An out-of-plane grating coupler for efficient butt-coupling between compact planar," *IEEE J. Quantum Electron.*, vol. 38, no. 7, pp. 949–955, Jul. 2002.

[24] W. Bogaerts, P. De Heyn, T. Van Vaerenbergh, K. De Vos, S. Kumar Selvaraja, T. Claes, P. Dumon, P. Bienstman, D. Van Thourhout, and R. Baets, "Silicon microring resonators," *Laser Photon. Rev.*, vol. 6, no. 1, pp. 47–73, Jan. 2012. [Online]. Available: http://doi.wiley.com/10.1002/lpor.201100017

[25] V. Ziebart, O. Paul, and H. Baltes, "Strongly buckled square micromachined membranes," *J. Microelectromech. Syst.*, vol. 8, no. 4, pp. 423–432, Dec. 1999. [Online]. Available: http://ieeexplore.ieee.org/lpdocs/epic03/wrapper.htm?arnumber=809057